Traffic noise prediction with the parabolic equation method: Validation of a split-step Padé approach in complex environments

Benoit Gauvreau[a] and Michel Bérengier[b]
Laboratoire Central des Ponts et Chaussées, Section Acoustique Routière et Urbaine, BP4129, 44341 Bouguenais Cedex, France

Philippe Blanc-Benon[c]
Ecole Centrale de Lyon, Laboratoire de Mécanique des Fluides et d'Acoustique, UMR CNRS 5509, BP 163, 69131 Ecully, France

Claude Depollier[d]
Institut d'Acoustique et de Mécanique, Université du Maine, BP 535, 72017 Le Mans, France

(Received 11 July 2001; revised 20 May 2002; accepted 26 May 2002)

This study deals with sound propagation in typical traffic noise conditions. The numerical results are obtained through the split-step Padé method and the discrete random Fourier modes technique. These are first evaluated *qualitatively*, by color contour maps showing noise propagation, diffraction by an impedance discontinuity or a screen edge, and scattering by atmospheric turbulence. Next, our numerical results are *quantitatively* validated by comparison with analytical models and other parabolic equation models. For all the atmospheric conditions and geometrical configurations available in literature, the agreement between the different methods is very good, except for some cases involving the atmospheric turbulence. However, in those particular cases, the split-step Padé results are shown to be more consistent with physical theory. Finally, our method seems to be very powerful and reliable for traffic noise prediction. © *2002 Acoustical Society of America.*
[DOI: 10.1121/1.1509074]

PACS numbers: 43.28.Js, 43.50.Vt [LCS]

I. INTRODUCTION

The present work focuses on traffic noise propagation, which often occurs above a plane and mixed ground (asphalt/grass) with topographical irregularities (barrier). The typical configuration and the parameters notations of this study are summarized in Fig. 1. The propagation medium (atmosphere) is either homogeneous or stratified, and eventually turbulent. We consider frequencies from 100 Hz to 5 kHz. This range is representative of the traffic noise spectrum, mainly generated by tire–road contact beyond 60 km/h. Experimental works carried out in the Laboratoire Central des Ponts et Chaussées (LCPC) showed that the equivalent sound source height is very low (of the order of a few centimeters, typically 3 cm) and that this source can be correctly modeled by a monopole.[1]

In recent past years, propagation of sound above a plane and heterogeneous ground in a homogeneous[2–9] or stratified[10] atmosphere has been extensively studied. In addition, other studies more specifically dealing with the introduction of an obstacle along the sound wave path in a homogeneous[11–18] or stratified[19–28] or turbulent[29,30] atmosphere have been carried out. When a noise barrier (or berm, slope, etc.) is located between the source and the receiver, an acoustic shadow zone appears behind the screen and can be reinforced for upward refraction. To obtain reliable predictions in this region, it is now well known that atmospheric turbulence must be taken into account.

The parabolic equation (PE) based methods seem to be the more appropriate ones, because of their ability to solve the problem of propagation above a mixed ground with topographical irregularities in a both refractive and turbulent atmosphere. Among these, the split-step Padé method[31] stands to be the more convenient within the framework of the traffic noise propagation, because of the good compromise between CPU time, accuracy in the heterogeneities location, and wide-angle properties.[32] Thus, in this paper, numerical results are obtained through the resolution of the parabolic equation with the split-step Padé method. The atmospheric turbulence is assumed to be only due to temperature fluctuations, and is numerically generated using the discrete random Fourier modes. Both theories are briefly reviewed in the following and then our model is validated. The split-step Padé results are first analyzed from a qualitative point of view: sound level contour maps effectively underline acoustic refraction, diffraction by an impedance discontinuity or a barrier edge, and scattering by atmospheric turbulence. Next, split-step Padé predictions are quantitatively compared to numerical, analytical, and experimental results already published for homogeneous and/or heterogeneous ground and/or atmosphere.

II. THE MODEL

In the linear acoustic approximation, the sound-pressure p is a solution of the elliptic Helmholtz propagation equation:

[a]Electronic mail: Benoit.Gauvreau@lcpc.fr
[b]Electronic mail: Michel.Berengier@lcpc.fr
[c]Electronic mail: Philippe.Blanc-Benon@ec-lyon.fr
[d]Electronic mail: Claude.Depollier@univ-lemans.fr

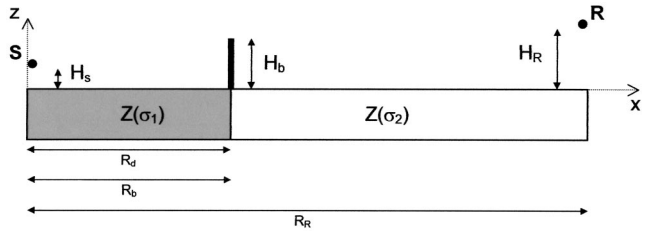

FIG. 1. Schematic representation and parameter notations.

$$\Delta p + k_0^2 p = 0, \tag{1}$$

where $k_0 = 2\pi f/c(z)n(z)$ is a reference wave number, f the frequency, c the sound speed, and n the refraction index. Assuming the azimuthal symmetry for the acoustic field, the sound-pressure $p(r,z)$ can be split into two components: a two-dimensional (2D) far field approximation for the Hankel function and a function $u(r,z)$ that is slowly range dependent. Then, assuming that the range dependence of the refraction index $n(r,z)$ is weak and neglecting the backscattering by index fluctuations, the acoustic field is dominated by forward propagating waves which are solutions of the one-way parabolic equation written in the 2D cylindrical coordinates system:[33]

$$\frac{\partial u(r,z)}{\partial r} = ik_0(Q-1)u(r,z), \tag{2}$$

where Q is the pseudo-differential operator defined as $Q^2 = 1+\xi+\eta$ with $\xi = (1/k_0^2)(\partial^2/\partial z^2)$ and $\eta = n^2 - 1$. Assuming that Q varies very slowly in the interval $[r_0, r_0+\Delta r]$, Eq. (2) can be directly integrated. This introduces an exponential operator[31] $\exp[\sigma(Q-1)]$, where $\sigma = ik_0\Delta r$. The next and major idea of the method is to approximate this exponential operator by a second-order Padé expansion of $Q = \sqrt{1+\xi+\eta} = \sqrt{1+\mathfrak{I}}$, which yields[34,35]

$$u(r_0+\Delta r,z) = \exp[\sigma(Q-1)]u(r_0,z) \approx \frac{1+p_1\mathfrak{I}+p_2\mathfrak{I}^2}{1+q_1\mathfrak{I}+q_2\mathfrak{I}^2}u(r_0,z), \tag{3}$$

where the coefficients p_1, p_2, q_1, and q_2 are easily deduced from a fourth-order Taylor series: $p_1 = (3+\sigma)/4$; $p_2 = (\sigma^2+6\sigma+3)/48$; $q_1 = (3-\sigma)/4$; $q_2 = (\sigma^2-6\sigma+3)/48$. Finally, the marching algorithm to obtain $u(r_0+\Delta r,z)$ from $u(r_0,z)$ is expressed in terms of the coefficients p_1, p_2, q_1, q_2, η and of the operator ξ, as

$$[1+q_1(\eta+\xi)+q_2(\eta+\xi)^2]u(r_0+\Delta r,z) = [1+p_1(\eta+\xi)+p_2(\eta+\xi)^2]u(r_0,z). \tag{4}$$

The numerical scheme deduced from Eq. (4) leads to a linear system with pentadiagonal matrices, solved at each step with a standard LU decomposition method.[36] Its stability is guaranteed by imposing that the denominator and the numerator elements of the rational approximation are complex conjugates of each other, so that the resulting rational function always has a modulus equal to unit. This second-order Padé scheme can accommodate very large included angles, which is really convenient for traffic noise propagation with acoustic barriers often close to the sound source.

The ground is modeled as a locally reacting surface with a complex impedance, which may change along the sound wave path. The impedance values are calculated from the air flow resistivity σ through the Delany and Bazley model.[37] We notice that, even if the impedance discontinuity and the barrier positions (R_d and R_b, rspectively, see Fig. 1) are set identical in the presented configurations, they are of course allowed to differ in our numerical code.

The mean vertical sound speed profiles are set constant along the distance and are logarithmically shaped as previously presented by Gilbert and White:[38]

$$c(z) = c_0 + a\ln(z/z_0), \tag{5}$$

where z_0 is the roughness parameter and "a" the refraction parameter.

A nonreflecting boundary condition is imposed at the top of the computational domain by adding an absorption layer of several wavelengths thickness, so that no significant acoustic energy is artificially introduced by reflection on the upper boundary of the waveguide.

The starting field required for the initialization of the marching algorithm has a Gaussian shape, an adjustable width, and takes into account the image source weighed by a complex reflection coefficient.

The atmospheric turbulence is considered as isotropic and homogeneous, and only due to temperature fluctuations. It is modeled by an averaging on N realizations of the refraction index, which random field is generated by a superposition of discrete random Fourier modes.[39] The turbulent energy spectrum (and thus the index fluctuations) depends on the choice of the turbulence spectrum, which profile is determined by the intensity μ_0^2 and the external (or macro) scale L_0 of turbulence. The Gaussian distribution is the most commonly used for modeling this turbulence spectrum.[40] However, except when indicated, we use a von Kàrmàn spectrum of the turbulent eddies.[41] The latter introduces an internal (or micro) scale of turbulence l_0. Its special domain is wider, and thus, better takes into account the turbulent eddies responsible for acoustic scattering in the atmosphere.[39]

The introduction of an acoustic barrier along the sound wave path is modeled by setting all the $u(r,z)$ to zero at the range step $r = R_b$ for $z \leqslant H_b$. This induces spurious oscillations due to numerical integration. Thus, as mentioned in Refs. 19 and 29, a spatial averaging is required to obtain smooth curves and reliable predictions. Moreover, it must be noticed that no diffraction coefficient has been considered in the PE code: the diffracted energy is only due to coupling between the equations in the linear system of Eq. (4).

The computation of the sound-pressure levels up to a distance of 1 km without turbulence is done with a grid spacing $\Delta r = \lambda/2$ and $\Delta z = \lambda/6$. On a SUN Ultra 10 360 MHz work station, the CPU time is 30 s for $f = 100$ Hz and 20 min for $f = 5$ kHz.

III. MAP ILLUSTRATIONS

A. Ground effects

For conciseness, we only present here results for 4 kHz, for heights up to 20 m and for distances up to 200 m. Other

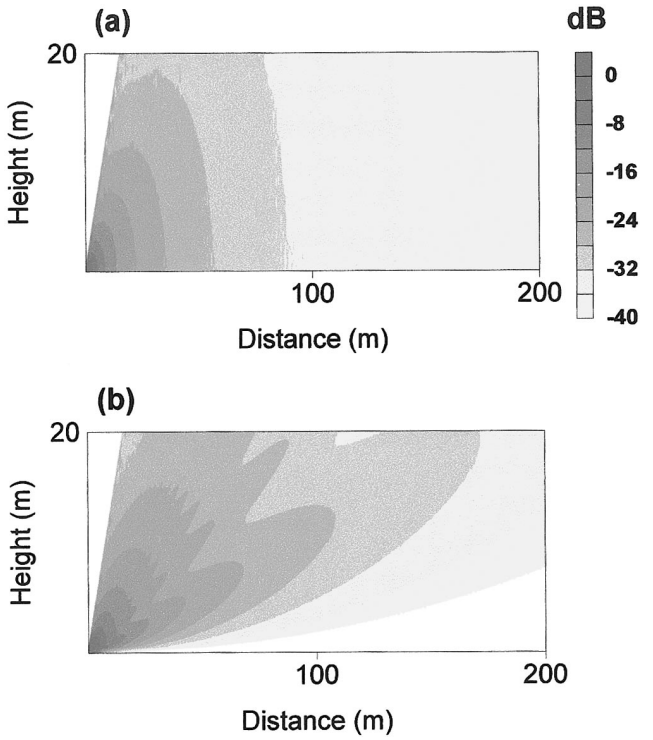

FIG. 2. Ground effects modeling. $f=4$ kHz; $H_S=10^{-2}$ m. (a): $\sigma_1=\sigma_2=3\times10^5$ kPa s m^{-2}. (b): $\sigma_1=3\times10^5$ kPa s m^{-2}; $\sigma_2=3\times10^2$ kPa s m^{-2}; $R_d=5$ m.

maps with higher sound source have clearly shown interference fringes, whose number increases with the frequency and with the source height.[32] In this part, the atmosphere is assumed to be homogeneous.

In Figs. 2(a) and (b), we plotted sound-pressure levels (SPLs) relative to a reference microphone installed close to the source. For both Figs. 2(a) and (b), the sound source elevation is 10^{-2} m, the frequency is 4 kHz, and the relative sound pressure level range $[-40$ dB; 0 dB$]$, with a color step each 4 dB. For a source very close to the ground ($H_S/\lambda \ll 1$) and for homogeneous and acoustically perfectly hard ground, no interference fringes occur and the propagation lobes turn to plane wave foreheads [Fig. 2(a)]. In Fig. 2(b), the air flow resistivity turns rapidly from 3×10^5 kPa s m^{-2} (sealed concrete for instance) to 3×10^2 kPa s m^{-2} (grass) 5 m from the source position. The introduction of an impedance jump leads to *diffraction* of the acoustic energy on this discontinuity, which then acts as a secondary source and which generates new propagation lobes [Fig. 2(b)]. We also verified that the main propagation lobes due to the impedance discontinuity are turned either upward or downward depending upon whether the sound speed gradient is, respectively, negative or positive.[23,32] In comparing Fig. 2(a) to Fig. 2(b), we also observe the intuitive phenomena that the ground absorption is reinforced and that the sound energy is considerably less important for the lowest receiver heights of the 2D waveguide. In both cases, the angular limitation of the method is easily visible.

B. Atmospheric effects

For a perfectly homogeneous and reflective ground, we specifically study the effects of the medium heterogeneities

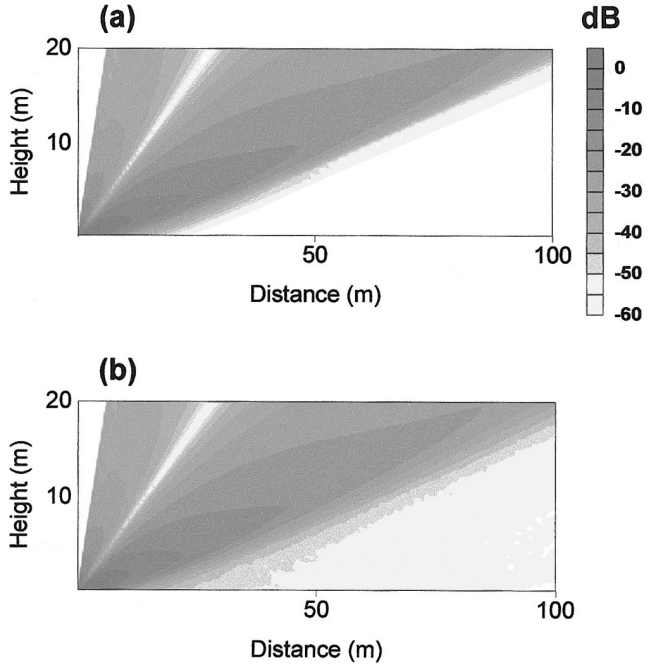

FIG. 3. Atmospheric effects modeling. Numerical predictions in the case of upward refraction for a nonturbulent (a) or turbulent (b) atmosphere. $f=5$ kHz; $H_S=0.03$ m; $\sigma_1=\sigma_2=3\times10^5$ kPa s m^{-2}; $a=-2$ m/s. von Kàrmàn spectrum (20 realizations); $\mu_0^2=8\times10^{-6}$; $L_0=1.1$ m; $I_0=0.05$ m.

on the sound propagation due to refraction and turbulence. The atmospheric turbulence has a stronger effect on the highest frequencies. This is the reason why Figs. 3(a) and (b) focus on the highest traffic noise frequency: 5 kHz. The source, surface, and atmosphere parameters values are indicated in figure captions.

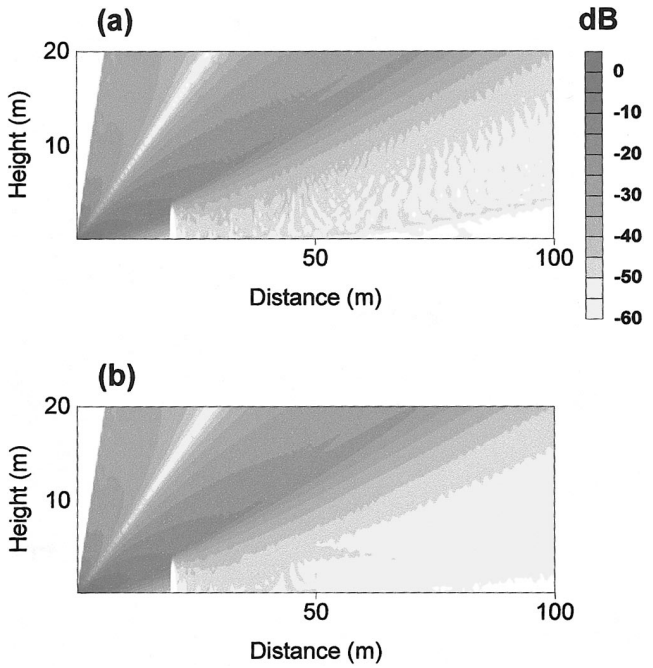

FIG. 4. Screen effects modeling. Numerical predictions in the case of upward refraction for a nonturbulent (a) or turbulent (b) atmosphere. $f=5$ kHz; $H_S=0.03$ m; $\sigma_1=\sigma_2=3\times10^5$ kPa s m^{-2}; $a=-2$ m/s; $R_b=20$ m; $H_b=4$ m. von Kàrmàn spectrum (20 realizations); $\mu_0^2=8\times10^{-6}$; $L_0=1.1$ m; $I_0=0.05$ m.

Temperature and wind vertical gradients induce vertical sound speed gradients, either positive or negative. In the first case ($a<0$ for downward refraction), interference fringes can even appear with very low source heights compared to the wavelength. These interference patterns are minimized by the decorrelation role of the atmospheric turbulence. Our method explicitly shows this phenomena in Refs. 30, 32, 34, and 35. In the second case ($a<0$ for upward refraction), an acoustic shadow zone appears. In this zone, relative sound-pressure levels theoretically decrease down to -60 dB, i.e., without turbulence [Fig. 3(a)]. The atmospheric turbulence enhanced the SPL in this region, by scattering the acoustic energy down to the ground. This is verified in Fig. 3(b).

C. Screen effects

We now introduce a thin screen along the sound wave path above a perfectly reflective ground. In the case of sound propagation for upward refraction, the effect of an acoustic barrier is reinforced: the diffraction fringes are turned upward as the diffraction lobes are in the presence of an impedance discontinuity,[23,32] and the acoustic shadow zone is even more emphasized. This is the most unfavorable situation for acoustic propagation [Fig. 4(a)].

When turbulence is considered [Fig. 4(b)], the sound levels behind the screen are not enhanced such as in an only *refractive* shadow zone [cf. Figs. 3(a) and (b)]. The preponderant mechanism responsible for the enhanced sound levels just behind the screen is the *diffraction* by its edge, and the sound field is almost *homogeneized* by the decorrelation role of turbulence. This implies a cancellation of the interference fringes between Figs. 4(a) and (b). For longer distances and for upward refraction, the *scattering* role of turbulence reappears and the relative contribution of diffraction and scattering to the sound spreading in the shadow region is inverted.

IV. QUANTITATIVE VALIDATION

The stability and the accuracy of the split-step Padé method have been tested for a large number of propagation conditions and frequencies.[32] In this part, the split-step Padé results are compared to those found in the literature for gradually more complex situations: homogeneous, heterogeneous, or screened ground, for a homogeneous, stratified, or turbulent atmosphere (except the case involving an impedance discontinuity in turbulent conditions, for which neither theoretical nor experimental data exist yet). Thus, we present sound-pressure levels calculated with our numerical code (SSP) under the same propagation conditions as detailed by the different authors. If there is no specific indication, the sound-pressure levels are relative to free field.

A. Homogeneous ground and atmosphere

In the trivial case that both the ground and atmosphere are homogeneous, we can compare the split-step Padé results with those given by PROPATE, a ray tracing alogirithm developed at the LCPC from Ref. 42 and largely validated by comparison with experimental data. In [100 Hz; 5 kHz] frequencies and [3×10^2 kPa s m^{-2}; 3×10^5 kPa m^{-2}] flow resistivities ranges, perfect agreement has been found for all

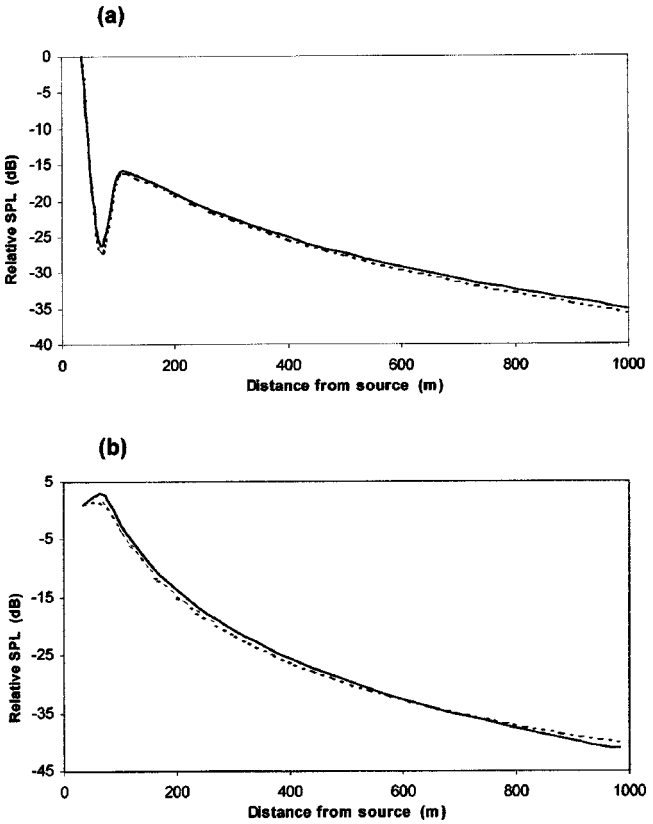

FIG. 5. Split-step Padé predictions (—) compared with ray method results (---) from PROPATE (Ref. 42). $f=5$ kHz; $H_S=H_R=1$ m. (a): $\sigma_1=\sigma_2=2\times10^5$ kPa s m^{-2}. (b): $\sigma_1=\sigma_2=3\times10^2$ kPa s m^{-2}.

cases. Figures 5(a) and (b) show two examples of SPL relative to a reference microphone, calculated with both methods for the highest traffic noise frequency 5 khz. The curves are always almost overlaying, including in destructive interference regions which appear when $H_S/\lambda\gg1$ and for high flow resistivity values [Fig. 5(a)].

B. Homogeneous ground-stratified atmosphere

SPL representation versus distance from the source position for a monochromatic acoustic sound wave in a stratified atmosphere has been treated by Galindo among others. She compared her PE calculations (CNPE) with Green's function parabolic equation and with fast field program predictions.[7] For distances from the sound source up to 1 km, the agreement was very satisfactory. Thus, her numerical results are used as *reference* data in these propagation conditions, involving homogeneous porous ground. In Figs. 6(a) and (b), we have plotted the relative SPL computed with our numerical code in the cases of, respectively, upward refraction ($a=-2$ ms^{-1}) and downward refraction ($a=+2$ ms^{-1}). Numerical data are obtained for $f=500$ Hz.

Figure 6(a) shows a rapid decay in the relative sound levels, as pronounced with the SSP predictions as with the CNPE ones. After 150 m, the relative level are less than -68 dB and strong oscillations occur, with a mean value nearly constant: this is identified with the acoustic shadow zone, where analytical theories do not predict any acoustic energy. In reality, we know that atmospheric turbulence scatters

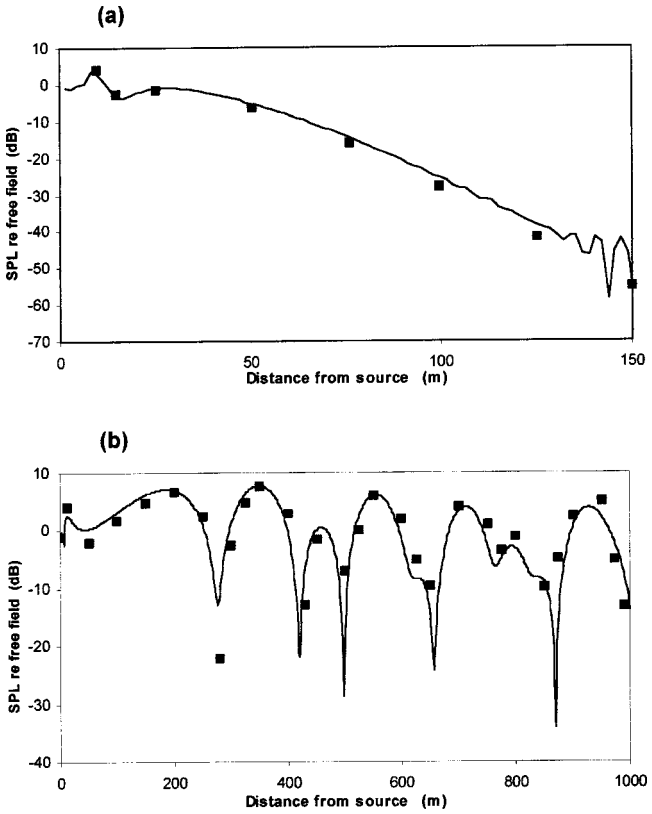

FIG. 6. Split-step Padé predictions (——) compared with CNPE results (■) from Galindo (Ref. 7). $f=500$ Hz; $H_S=1.5$ m; $H_R=2$ m; $\sigma_1=\sigma_2=2\times10^2$ kPa s m^{-1}. (a) Upwind conditions, $a=-2$ m/s, (b) downwind conditions, $a=+2$ m/s.

acoustic energy in this region. When distance and frequency increase, the introduction of these effects is necessary to obtain reliable numerical predictions. It will be discussed later in this paper.

In downwind conditions [Fig. 6(b)], the predictions obtained with the two numerical methods are identical for distances up to 1 km: the respective relative SPL values are very close to each other, except in the destructive interference regions. A slight difference appears in those values and increases with the distance. The nature of these errors has been presented by Galindo in terms of a *level* error introduced by the selection of the starting field, and of a *phase* error generated by the rational linear approximation [Eq. (3)] and worsened in strong downward refraction conditions.[7,43]

C. Homogeneous ground-turbulent atmosphere

The first effect of atmospheric turbulence on acoustic field is decorrelation of coherent wave front, which minimizes destructive interferences and which smooths sound level profiles when $H_S/\lambda \gg 1$, or for downward refraction ($a>0$), or if the surface is concave. In Refs. 32, 34, and 35, good agreement has been found between split-step Padé predictions and Daigle's experimental data[44] for those propagation situations.

The sound effect of turbulence is scattering of sound energy downward into the shadow region when we consider propagation above a convex surface or for upward refraction ($a<0$). This latter case is studied in Fig. 7. We plot SSP

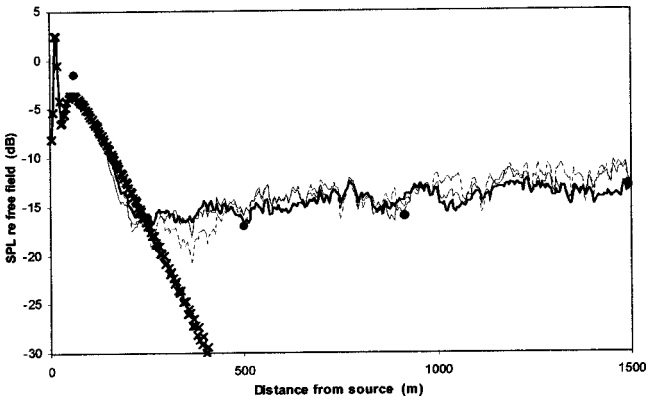

FIG. 7. Split-step Padé predictions in deterministic (×) or turbulent cases: (---) 10 realizations; (——) 20 realizations; (—) 40 realizations compared with experimental data (●) from Wiener and Keast (Ref. 45). $f=424$ Hz; $H_S=1.2$ m; $H_R=0.6$ m; $\sigma_1=\sigma_2=3\times10^2$ kPa s m^{-2}; $a=-0.5$ m/s. von Kàrmàn spectrum; $\mu_0^2=7.7\times10^{-6}$; $L_0=1.1$ m; $l_0=0.05$ m.

predictions with and without turbulence in the same propagation conditions as in the Wiener and Keast experiments.[45] For nonturbulent conditions, the relative SPL predictions rapidly decrease, whereas turbulent predictions are very close to the experimental values. Turbulent results are indicated for three different numbers of realizations, in order to give an idea of their convergence. The slight discrepancy between experimental and numerical results can be explained in terms of uncertainty in the acoustic, climatic, and impedance measurements. However, the relative SPL profiles are very similar as far as turbulence is considered.

D. Impedance discontinuity-homogeneous atmosphere

Craddock and White[2] have first introduced an impedance discontinuity in a numerical code based on the PE (finite differences with the Cranck–Nicolson scheme—CNPE). They validated their results by comparing them with analytical models predictions, in particular one from Rasmussen.[46] They next chose a SPL representation versus distance (and thus for a fixed frequency) to illustrate in a better way the jump in the impedance values, but for which there were neither experimental nor numerical data available for comparison. Their results for either a homogeneous and perfectly reflective ground or heterogeneous hard/soft ground are plotted in Fig. 8 and compared to split-step Padé results for the same cases. We also mentioned in Fig. 8 the results given by an analytical model developed at the LCPC and based on Rasmussen's technique.[46]

The agreement between the three methods is excellent, except in the destructive interference region where the sound-pressure levels dramatically fall and where the accuracy in the grid spacing is of great importance.

E. Impedance discontinuity-stratified atmosphere

For this more complex situation involving a sound wave propagating above a heterogeneous ground (without screen) through a stratified atmosphere, only upward refraction cases exist in the literature. In Ref. 10, Bérengier and Daigle compared indoor experimental data obtained for propagation of

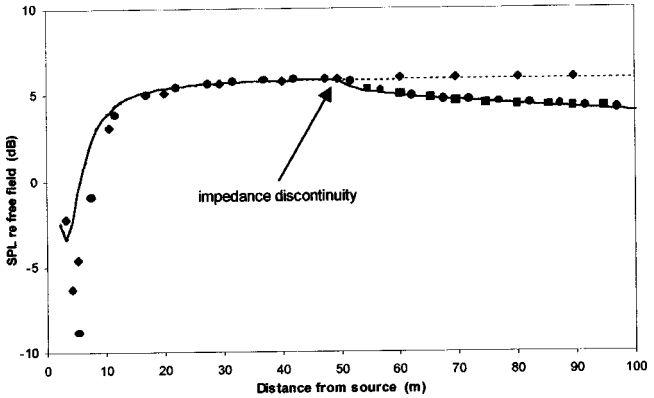

FIG. 8. Split-step Padé predictions for a homogeneous (---) and heterogeneous (——) ground compared with CNPE results from Craddock and White (Ref. 2) in the same conditions (♦ and ■, respectively). Also plotted: results from Rasmussen model (Ref. 46) for heterogeneous ground (●). $f=160$ Hz; $H_S=1.5$ m; $H_R=1.8$ m; $\sigma_1=2\times10^5$ kPa s m^{-2}; $\sigma_2=2\times10^2$ kPa s m^{-2}; $R_d=50$ m.

sound above a curved surface having an impedance discontinuity, with analytical predictions given by a residue series solution. Assuming a far field approximation in our PE method, we proceed to a scale change in order to correctly compare our results to Bérengier and Daigle's data (Fig. 9). We thus multiply by 10 the geometrical parameters, and divide by 10 the frequency and the air flow resistivity.

In Fig. 9, the shorter range split-step Padé results provide a better fit to experimental data than Bérengier and Daigle's analytical predictions. According to the authors, this deviation beyond the discontinuity could be explained by the choice of the edge diffraction coefficient $D=1$ in their model.[10] The discrepancy between the split-step Padé calculations and the experimental acquisitions at ''long'' distances could be attributed, in one part, to the inaccuracy in the experimental air flow resistivity measurement and, in another part, to the impedance discontinuity location. This last point is amplified by the scale factor and by the very strong linear gradient value, due to the analogy between sound propagation in a homogeneous atmosphere above a curved surface and sound propagation in a stratified atmosphere above a plane surface.[10]

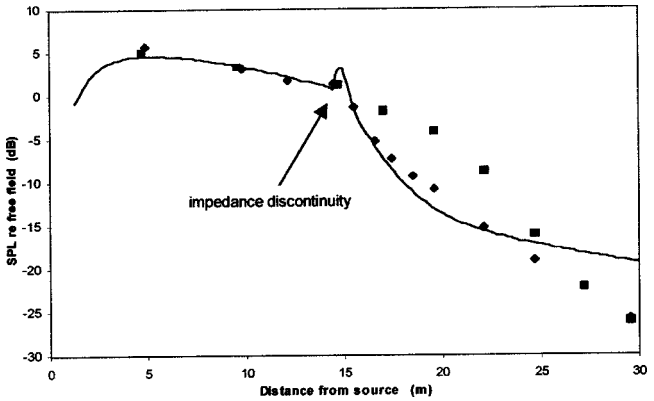

FIG. 9. Split-step Padé predictions (——) compared with experimental (♦) and theortical (■) results from Bérengier and Daigle (Ref. 10). $f=400$ Hz; $H_S=H_R=0.5$ m; $\sigma_1=5\times10^4$ kPa s m^{-2}; $\sigma_2=50$ kPa s m^{-2}; $R_d=15$ m. $a=-68.8$ m/s (linear gradient until the altitude $z=1.2$ m).

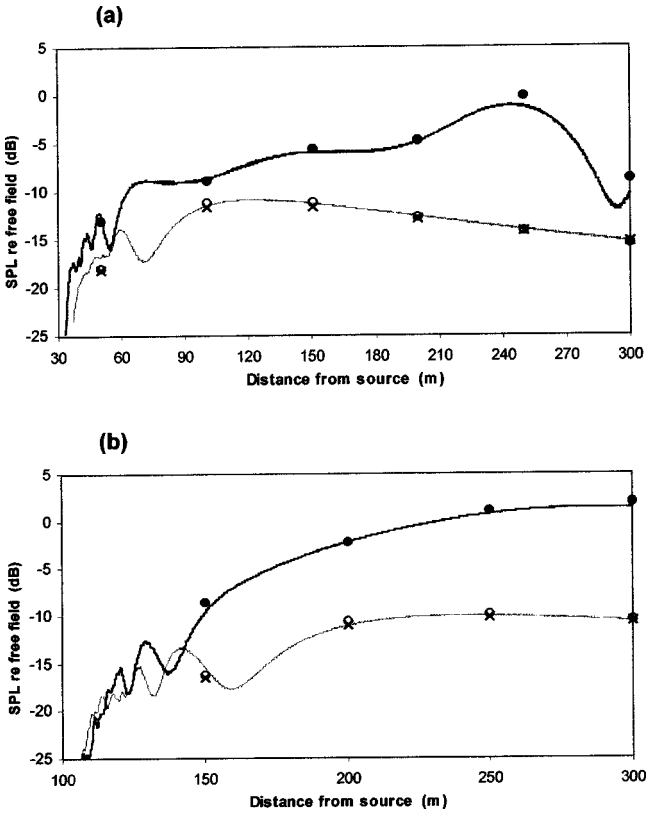

FIG. 10. Split-step Padé predictions for $a=0$ m/s (thin line) and $a=2$ m/s (thick line) compared with Salomons predictions (Ref. 19) for the same values (○ and ●, respectively), and those from Hadden and Pierce—Ref. 47 (×) for a homogeneous atmosphere ($a=0$ m/s). $f=1$ kHz; $H_S=H_R=2$ m; $\sigma_1=\sigma_2=3\times10^2$ kPa s m^{-2}. (a) $R_b=30$ m; $H_b=4$ m. (b) $R_b=100$ m; $H_b=6$ m.

F. Acoustic barrier-homogeneous and stratified atmosphere

The predicted results are directly compared to those from Salomons[19] in a downward refracting and nonturbulent atmosphere, for the same physical parameters values (see captions) and for identical screen locations and dimensions: $R_b=30$ m, $H_b=4$ m [Fig. 10(a)] and $R_b=100$ m, $H_b=6$ m [Fig. 10(b)]. In each figure, we plot as a reference Hadden and Pierce's analytical predictions, given for a homogeneous atmosphere and an absorbent barrier.[47] It must be emphasized that no diffraction coefficient has been considered in our PE code: the diffracted energy is only due to coupling in the linear system of Eq. (4). The agreement between the various models is very good for all the propagation conditions and geometrical configurations, except just downstream from the screen, where some oscillations occur in the relative SPL due to numerical instabilities in the PE solution just behind the screen edge [Figs. 10(a) and (b)].

G. Acoustic barrier-homogeneous and turbulent atmosphere

Now, the split-step Padé results are compared to those from Forssén[29] for a turbulent but nonstratified atmosphere, and for the frequencies $f=500$ Hz [Figs. 11(a) and (b)] and $f=1$ kHz [Figs. 12(a) and (b)]. They are calculated with an averaging on 10 realization, using a Gaussian spectrum for

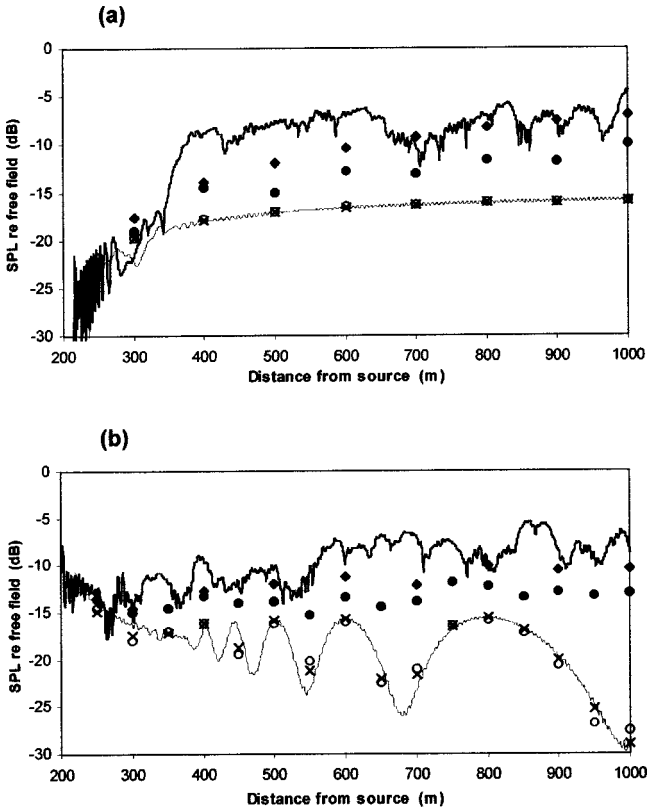

FIG. 11. Split-step Padé predictions for a homogeneous (thin line) and turbulent (thick line) atmosphere compared with Forssén predictions (Ref. 29) for the same values (○ and ●, respectively). Also plotted: results from the Hadden and Pierce model (Ref. 47) for a homogeneous atmosphere (×) and results from the Daigle model (Ref. 48) for a turbulent atmosphere (◆). $f=500$ Hz; $H_S=0$ m; $\sigma_1=\sigma_2=3\times10^5$ kPa s m^{-2}; $R_b=200$ m; $H_b=20$ m; Gaussian distribution (10 realizations); $\mu_0^2=3\times10^{-6}$; $L=1.1$ m. (a) $H_R=0$ m. (b) $H_R=20$ m.

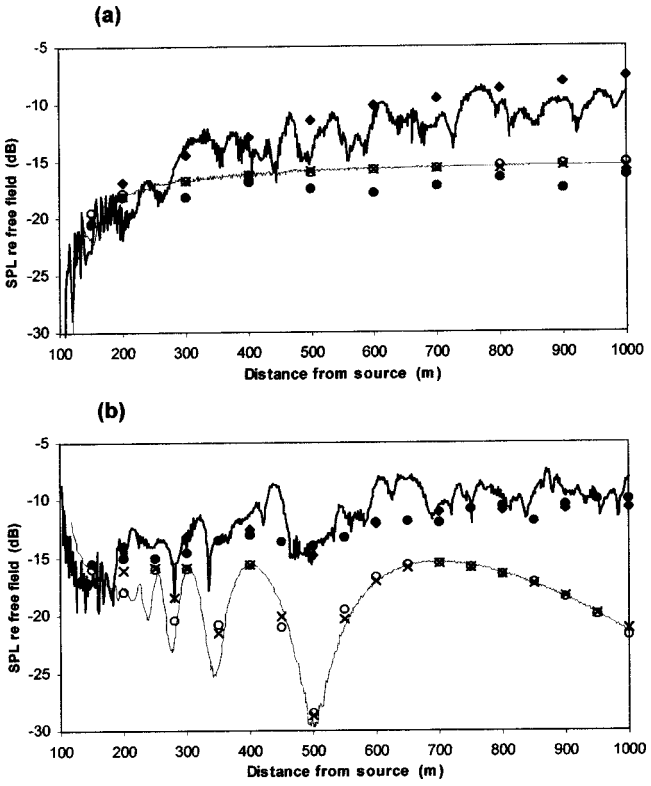

FIG. 12. Split-step Padé predictions for a homogeneous (thin line) and turbulent (thick line) atmosphere compared with Forssén predictions (Ref. 29) for the same values (○ and ●, respectively). Also plotted: results from the Hadden and Pierce model (Ref. 47) for a homogeneous atmosphere (×) and results from the Daigle model (Ref. 48) for a turbulent atmosphere (◆). $f=1000$ Hz; $H_S=0$ m; $\sigma_1=\sigma_2=3\times10^5$ kPa s m^{-2}; $R_b=100$ m; $H_b=10$ m; Gaussian distribution (10 realizations); $\mu_0^2=3\times10^{-6}$; $L=1.1$ m. (a) $H_R=0$ m. (b) $H_R=10$ m.

the turbulence as the author did. In this case again, the Hadden and Pierce calculations for a homogeneous atmosphere and an absorbent barrier are indicated as a reference. In the turbulent cases, we also plot predictions given by Daigle's model, which uses diffraction and scattering cross section theories.[48] The relative SPLs existing *behind the screen* are given for receiver heights $H_R=0$ m [Figs. 11(a) and 12(a)] and $H_r=H_b$ [Figs. 11(b) and 12(b)]. Location and dimension of the barrier are, respectively, $R_b=200$ m and $H_b=20$ m for Fig. 11, and $R_b=100$ m and $H_b=10$ m for Fig. 12.

In deterministic cases, the three methods (split-step Padé, Forssén, Hadden, and Pierce) give exactly the same results, except immediately behind the screen as previously explained. When $H_R/\lambda \ll 1$, no interference occurs, and the relative SPL tends toward an asymptotic limit [Figs. 11(a) and 12(a)]. For higher receivers, interference fringes appear where the different methods give very similar predictions [Figs. 11(b) and 12(b)].

In order to limit the variation parameter number in the turbulent cases, we use a *Gaussian* distribution for the index fluctuations as Forssén did. Generally speaking, our results are very close to Daigle's and slightly stronger than Forssén's. As mentioned by Forssén[29] by comparison with Daigle's model, Forssén's predictions sometimes underestimate the sound-pressure levels existing in the shadow zone [Fig. 12(a)]. On the contrary, the discrete random Fourier modes technique predicts more enhanced sound levels in this region and demonstrates again its efficiency and its accuracy.

V. CONCLUSION

The split-step Padé method coupled with the discrete random Fourier modes technique have been validated for a large number of propagation configurations. Qualitatively, sound maps illustrated propagation mechanisms in the presence of a monopole source very close to the ground, an impedance discontinuity, an acoustic barrier, and a stratified or turbulent atmosphere.

Then, sound-pressure levels computed with the split-step Padé method were compared with relevant data from the literature. The quantitative agreement is generally very good, without introducing any additional heuristic coefficient in screened configurations. Thus, our PE-based method appears to be reliable to predict traffic noise propagation in such complex environments.

This work opens the field for further investigations, notably the more precise description of sound speed profiles in the vicinity of multishaped obstacles. Outdoor controlled experiments have been realized in order to validate the code for such complex configurations, for which no data exist yet. This will be the subject of a further paper.

[1] J. F. Hamet, M. A. Pallas, D. Gaulin, and M. Bérengier, ''Acoustical modeling of road vehicles for traffic noise predictions: Determination of the source height,'' 16th ICA-ASA Congress, Seattle, USA, J. Acoust. Soc. Am. **103**, 2919 (1998).
[2] J. M. Craddock and M. J. White, ''Sound propagation over a surface with varying impedance: A parabolic equation approach,'' J. Acoust. Soc. Am. **91**, 3184–3191 (1992).
[3] K. B. Rasmussen, ''Scale model simulation of sound propagation over an impedance discontinuity,'' Proceedings of Inter-Noise **93**, 1711–1714 (1993).
[4] M. Galindo, ''Application of the parabolic approximation method to sound propagation above ground with impedance variations,'' Proceedings of the Sixth International Symposium on Long Range Sound Propagation, Ottawa, Canada, 12–14 June 1994, pp. 394–407.
[5] D. C. Hothersall and J. N. B. Harriott, ''Approximate models for sound propagation above multi-impedance plane boundaries,'' J. Acoust. Soc. Am. **97**, 918–926 (1995).
[6] J. S. Robertson, P. J. Schlatter and W. L. Siegmann, ''Sound propagation over impedance discontinuities with the parabolic approximation,'' J. Acoust. Soc. Am. **99**, 761–767 (1996).
[7] M. Galindo, ''The parabolic equation method for outdoor sound propagation,'' Ph.D. thesis, Technical University of Denmark, 1996.
[8] M. R. Stinson and G. A. Daigle, ''Surface wave formation at an impedance discontinuity,'' J. Acoust. Soc. Am. **102**, 3269–3275 (1997).
[9] P. Boulanger, T. Waters-Fuller, K. Attenborough, and K. M. Li, ''Models and measurements of sound propagation from a point source over mixed impedance ground,'' Proceedings of the Seventh International Symposium on Long Range Sound Propagation, Lyon, France, 24–26 July 1996, pp. 291–305.
[10] M. Bérengier and G. A. Daigle, ''Diffraction of sound above a curved surface having an impedance discontinuity,'' J. Acoust. Soc. Am. **84**, 1055–1060 (1988).
[11] Y. W. Lam and S. C. Roberts, ''A simple method for accurate prediction of finite barrier insertion loss,'' J. Acoust. Soc. Am. **93**, 1445–1452 (1993).
[12] D. J. Saunders and R. D. Ford, ''A study of the reduction of explosive impulses by finite sized barriers,'' J. Acoust. Soc. Am. **94**, 2859–2875 (1993).
[13] K. B. Rasmussen, ''Model experiments related to outdoor propagation over an earth berm,'' J. Acoust. Soc. Am. **96**, 3617–3620 (1994).
[14] E. M. Salomons, ''Sound propagation in complex outdoor situations with a non-refracting atmosphere: Model based on analytical solutions for diffraction and reflection,'' Acustica **83**, 436–454 (1997).
[15] S. S. T. Ho, I. J. Busch-Vishniac, and D. T. Blastock, ''Noise reduction by a barrier having a random edge profile,'' J. Acoust. Soc. Am. **101**, 2669–2676 (1997).
[16] M. Salomons, A. C. Geerlings, and D. Duhamel, ''Comparison of a ray model and a Fourier-boundary element method for traffic noise situations with multiple diffractions and reflections,'' Acustica **83**, 35–47 (1997).
[17] J. P. Chambers, G. J. Wadsworth, M. Kelly, and R. Raspet, ''Scale model experiments on the insertion loss of wide and double barriers and barriers under turbulent conditions,'' Proceedings of the Eighth International on Long Range Sound Propagation, Penn State College, 1998, pp. 153–167.
[18] J. S. Robertson, ''Sound propagation over a large wedge: A comparison between the geometrical theory of diffraction and the parabolic equation,'' J. Acoust. Soc. Am. **106**, 113–119 (1999).
[19] E. M. Salomons, ''Diffraction by a screen in downwind sound propagation: A parabolic equation approach,'' J. Acoust. Soc. Am. **95**, 3109–3117 (1994).
[20] K. B. Rasmussen, ''Sound propagation over screened ground under upwind conditions,'' J. Acoust. Soc. Am. **100**, 3581–3586 (1996).
[21] E. M. Salomons, ''Noise barriers in a refracting atmosphere,'' Appl. Acoust. **47**, 217–238 (1996).
[22] K. B. Rasmussen and M. Galindo Arranz, ''The insertion loss of screens under the influence of wind,'' J. Acoust. Soc. Am. **104**, 2692–2698 (1998).
[23] B. Gauvreau, M. Bérengier, Ph. Blanc-Benon, and C. Depollier, ''Impedance discontinuity and range dependent refraction profile: A numerical study,'' in Ref. 17, pp. 225–240.
[24] K. M. Li and Q. Wang, ''A BEM approach to assess the acoustic performance of noise barriers in a refracting atmosphere,'' J. Sound Vib. **211**, 663–681 (1998).
[25] S. Taherzadeh, K. M. Li, and K. Attenborough, ''Sound propagation in a refracting medium above an uneven terrain,'' in Ref. 17, pp. 101–111.
[26] N. Barriere and Y. Gabillet, ''Sound propagation over a barrier with realistic wind gradients. Comparison of wind tunnel experiments with GFPE computations,'' Acustica **85**, 325–334 (1999).
[27] D. Zhu, ''Use of the parabolic equation method for predictions of outdoor sound propagation in complex environments,'' Proceedings of the Sixth International Congress on Sound and Vibration, Copenhagen, Denmark, 1999, pp. 669–676.
[28] E. M. Salomons, ''Reduction of the performance of a noise screen due to screen-induced wind-speed gradients. Numerical computations and wind-tunnel experiments,'' J. Acoust. Soc. Am. **105**, 2287–2293 (1999).
[29] J. Forssén, ''Calculation of sound reduction by a screen in a turbulent atmosphere using the parabolic equation method,'' Acustica **84**, 599–606 (1998).
[30] B. Gauvreau, M. Bérengier, Ph. Blanc-Benon, and C. Depollier, ''A numerical method to predict sound propagation for realistic road environments,'' J. Acoust. Soc. Am. **105**, 1335(A) (1999).
[31] M. D. Collins, ''A split-step Padé solution for the parabolic equation method,'' J. Acoust. Soc. Am. **93**, 1736–1742 (1993).
[32] B. Gauvreau, ''Influence des conditions micrométéorologiques sur l'efficacité des écrans acoustiques,'' Ph.D. thesis, Université du Maine, Le Mans, France, 1999.
[33] F. D. Tappert and R. H. Hardin, ''Computer simulation of long-range ocean acoustic propagation using the parabolic equation method,'' Proceedings of the Eighth International Congress on Acoustics, 1974, p. 452.
[34] P. Chevret, ''Simulation numérique des effets de la turbulence atmosphérique sur la propagation du son dans l'atmosphère,'' Ph.D. thesis, Ecole Centrale de Lyon, France, 1994, No. 94-18.
[35] P. Chevret, Ph. Blanc-Benon, and D. Juvé, ''A numerical model for sound propagation through a turbulent atmospheres near the ground,'' J. Acoust. Soc. Am. **100**, 3587–3599 (1996).
[36] W. H. Press, B. P. Flannery, S. A. Teukolsky, and W. T. Vetterling, *Numerical Recipes* (Cambridge University Press, Cambridge, 1992).
[37] M. E. Delany and E. N. Bazley, ''Acoustical properties of fibrous absorbent materials,'' Appl. Acoust. **3**, 105–116 (1970).
[38] K. E. Gilbert and M. J. White, ''Application of the parabolic equation to sound propagation in a refracting atmosphere,'' J. Acoust. Soc. Am. **85**, 630–637 (1989).
[39] D. Juvé, Ph. Blanc-Benon, and P. Chevret, ''Numerical simulation of sound propagation through a turbulent atmosphere,'' Proceedings of the Fifth International Symposium on Long Range Sound Propagation, Milton Keynes, UK, 24–26 May 1992, pp. 282–296.
[40] G. A. Daigle, J. E. Piercy, and T. F. W. Embleton, ''Line-of-sight propagation through atmospheric turbulence near the ground,'' J. Acoust. Soc. Am. **74**, 1505–1513 (1983).
[41] A. Ishimaru, *Wave Propagation and Scattering in Random Media* (Academic, New York, 1978), Vol. 2.
[42] J. E. Piercy, T. F. W. Embleton, and L. C. Sutherland, ''Review of noise propagation in the atmosphere,'' J. Acoust. Soc. Am. **61**, 1403–1418 (1977).
[43] M. Galindo, ''Approximations in the PE method. Phase and level errors in a downward refracting atmosphere,'' Proceedings of the Seventh International Symposium on Long Range Sound Propagation, Lyon, France, 1996, pp. 235–255.
[44] G. A. Daigle, J. E. Piercy, and T. F. W. Embleton, ''Effects of atmospheric turbulence on the interference of sound waves near a hard boundary,'' J. Acoust. Soc. Am. **64**, 622–630 (1978).
[45] F. M. Wiener and D. N. Keast, ''Experimental study of the propagation of sound over ground,'' J. Acoust. Soc. Am. **31**, 724–733 (1959).
[46] K. B. Rasmussen, ''A note on the calculation of sound propagation over impedance jumps and screens,'' J. Sound Vib. **84**, 598–602 (1982).
[47] W. J. Hadden and A. D. Pierce, ''Sound diffraction around screens and wedges for arbitrary point source locations,'' J. Acoust. Soc. Am. **69**, 1266–1276 (1981). Erratum **71**, 1290 (1982).
[48] G. A. Daigle, ''Diffraction of sound by a noise barrier in the presence of atmospheric turbulence,'' J. Acoust. Soc. Am. **71**, 847–854 (1982).